Water Practice & Technology

IWA PUBLISHING

Water Practice & Technology Vol 16 No 4, 1475 doi: 10.2166/wpt.2021.081

Kinetics, isotherm and thermodynamic studies of S^{2-} adsorption by (SBA-15)-Hg (II)

Xiao-Dong Li[a] and Qing-Zhou Zhai[b,*]

[a] Department of Basic Science, Jilin Jianzhu University, 5088 Xincheng Street, Changchun, Jilin Province 130118, China
[b] Research Center for Nanotechnology, Changchun University of Science and Technology, 7186 Weixing Road, Changchun 130022, China
*Corresponding author. E-mail: zhaiqingzhou@163.com

ABSTRACT

The nano-mesoporous material SBA (Santa Barbara Amorphous)-15 was synthesized using the hydrothermal method. Hg^{2+} was adsorbed by SBA-15 and then the S^{2-} in the aqueous phase by (SBA-15)-Hg(II), with the hope that materials with better S^{2-} adsorption properties can be obtained. The relevant materials were characterized by X-ray diffraction, scanning electron microscopy, 77 K nitrogen adsorption-desorption, and related product characteristics were determined. In this work, the adsorption conditions of S^{2-} onto (SBA-15)-Hg(II) were optimized. Adsorption efficiency reached about 92% and the adsorption capacity 55.02 mg/g. Studies of the system's adsorption kinetics showed that the pseudo-second-order equation applies. The thermodynamic results indicated that $\Delta G^0 < 0$, $\Delta H^0 = -28.56$ kJ/mol, $\Delta S^0 = -81.136$ J/(mol·K), and that adsorption is exothermic, enthalpy decreases and the reaction is spontaneous. This accords with the Freundlich isothermal adsorption equation.

Key words: adsorption, Hg^{2+}, mesoporous material, SBA-15, S^{2-}

HIGHLIGHTS

- Under the optimized adsorption conditions, the adsorption rate of S^{2-} reached 92% and the adsorption capacity reached 55.02 mg/g.
- The adsorption process of S^{2-} by the (SBA-15)-Hg(II) is in accordance with the quasi-second-order kinetic equation in kinetic aspect, and the adsorption isotherm is in accordance with the Freundlich model.

GRAPHICAL ABSTRACT

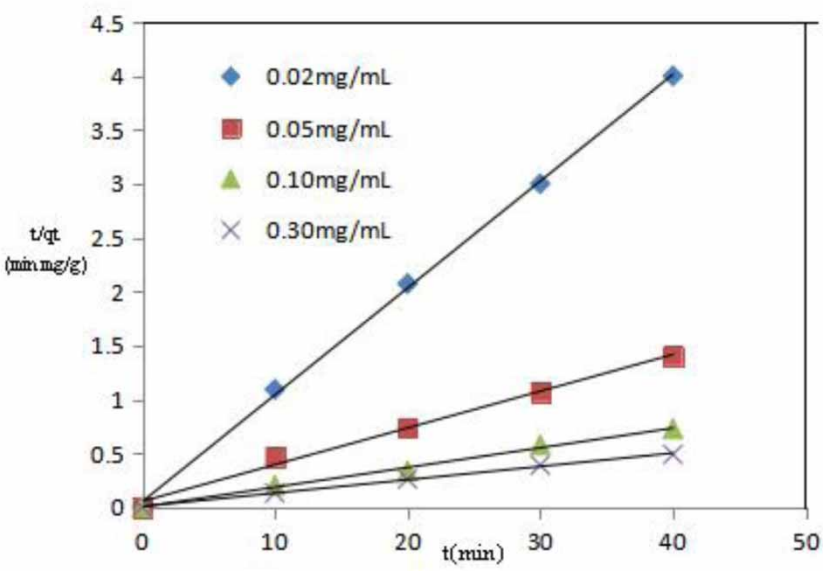

1. INTRODUCTION

With the steady development of industrialization, the effect of anthropogenic activities on the environment is becoming more and more serious, and environmental pollution has become a major threat (Diagboya & Dikio

2018; Nazal *et al.* 2021; Wu *et al.* 2021). Wastewater treatment is a major problem in relation to a wide range of environmental pollution.

Sulfur-containing sewage is an important source of pollution, mainly from species such as hydrogen sulfide and sodium sulfide. The direct source of sulfide sewage is industrial wastewater discharges, and the indirect source is the reduction of sulfate in the sewage to sulfide. Conversion by microorganisms is also an important source of sulfur-containing wastewater. Industrial activities such as oil refining, paper-making, printing and leather manufacture all produce sulfide-containing wastewaters.

Industrial wastewater containing high sulfur concentrations is highly corrosive, and can damage plant roots and thus affect plant growth. If the sulfide concentration in water exceeds 0.07 μg-S/L, the water will have a peculiar smell, and when it reaches 0.15 μg-S/L, it affects the growth of fish fry and egg. At the same time, the dissolved sulfide can also be degraded to hydrogen sulfide and diffuse into the atmosphere. Hydrogen sulfide, which smells like rotten eggs, is harmful – that is, toxic – and excessive inhalation can have a variety of effects on body functions including the respiratory, digestive and circulatory systems, and so on (Wang & Hu 2006; Chang *et al.* 2018).

Because of these various problems, it is necessary to process sulfur-containing sewage before discharge to the environment. Various treatment methods have been adopted to control this kind of pollution, including membrane separation, ion exchange, activated sludge, chemical reactions, and so on (Wang & Hu 2006). However, they are inconvenient and expensive to use, and some produce new liquid and/or solid wastes, resulting in secondary pollution and operating inconvenience.

The use of adsorbents for pollution control is quick. Adsorption technology has practical value because of its simple operation and low cost, and the cost-performance, which is better than other water pollution treatment methods. Activated carbon is a traditional absorbent, and while its adsorption performance is excellent its regeneration is difficult and costly (Diagboya & Dikio 2018).

Compared with traditional adsorbents, nanomaterials have high specific surfaces and chemical activity, giving them more advantages as adsorbents than other materials and can lead to better adsorption effects. Adsorption can be used to remove sulfur ions selectively from wastewater, and the sulfur removed cannot migrate into the environment or, therefore, make it worse. However, due to the sulfur ions' own properties, traditional adsorption technology cannot deal effectively with sulfur-containing materials. It is an important solution and technical challenge, therefore, to study materials that adsorb sulfur strongly, and apply them to the treatment of sulfur containment.

Porous zeolite adsorbents are modern and efficient, and their high surface activity can provide a good base for their modification. The zeolite molecular pore channel is long, its specific surface is large, and it has good adsorption properties. Compared with microporous molecular sieves, the mesoporous molecular sieve pore size and specific surface are larger, and it should also have better adsorption properties.

SBA-15 is an excellent mesoporous material with a pore size range of 4.6–30 nm, and has one of the largest pore diameters among mesoporous materials. The specific surface is large, and the thermostabilization performance is good (Castillo *et al.* 2018; Dido *et al.* 2018; Kanga *et al.* 2018; Pirez *et al.* 2018; Mikheeva *et al.* 2019; Szewczyk *et al.* 2019; Zhai 2020). The main raw material for making SBA-15 is silicon – that is a mixture of silicon and oxygen – which makes its framework relatively inactive leading, in turn, to a reduction in its ion-exchange capacity. In order to deal with this defect in SBA-15, its properties are changed by adding metal ions to the material's skeleton by sorption. This type of modification can not only improve the material's hydrothermal stability but also make up its lattice defects and enhance its ability to participate in chemical reactions, all of which influence the application of SBA-15 significantly (Lakhi *et al.* 2018).

In this work, an SBA-15 nano-mesoporous molecular sieve was synthesized. The experimental conditions for Hg^{2+} adsorption by SBA-15 are described elsewhere (Zhai *et al.* 2011) and the optimized adsorption conditions S^{2-} by (SBA-15)-Hg(II) were studied in the work described here. The adsorption kinetics, thermodynamics and adsorption isotherm properties were studied and their related adsorption properties were found. The material can adsorb not only Hg^{2+} but also S^{2-}.

2. EXPERIMENT

2.1. Reagents

The reagents triblock copolymer, polyethylene glycol-block-polypropylene glycol-block-poly(ethylene glycol) (P123, Aldrich), tetraethoxysilane (TEOS, Shanghai First Plant of Reagent, China), hydrochloric acid (12 mol/L,

Beijing Chemical Plant, China), sodium sulfide ($Na_2S{\cdot}9H_2O$, Beijing Chemical Plant, China), $Hg(NO_3)_2{\cdot}0.5H_2O$ (Tianjin Guangfu Fine Research Institute of Chemical Engineering, China), and silver nitrate and sodium hydroxide (both Beijing Chemical Plant) were used. All reagents were analytical grade. Deionized water was used.

2.2. Instruments

Powder X-ray diffraction (XRD) analysis was done using a D5005 diffractometer (Siemens, Germany) using Cu-K_α. The x-ray wavelength, λ, was 1.5418 Å, operating (tube) voltage 40 kV, and operating (tube) current 30 mA with scanning range 0.4–6° and step size 0.02°.

Particle morphology and size were obtained on a scanning electron microscope (Philips XL30) running at 20 kV.

The nitrogen adsorption-desorption results were determined using a Micromeritics Corporation (USA) ASAP 2020 V3.01 H-type adsorption analyzer at 77 K. Samples were vacuum-activated at 363 K for 12 hours and the data calculated using the BdB (Broekhoff and de Boer) method (Broekhoff *et al.* 1968a, 1968b).

The specific surface was analyzed and calculated by the BET (Brunauer-Emmett-Teller) method (Brunauer *et al.* 1938), and the pore size distribution by the BJH (Barrett–Joyner-Halenda) method (Barrett *et al.* 1951).

2.3. Experimental methods

2.3.1. Synthesis of mesoporous molecular sieve SBA-15

Mesoporous molecular sieve SBA-15 was synthesized by the hydrothermal method (Zhai 2012). 2 g of P123 template were dissolved in 15 mL of deionized water and 60 g of 2 mol/L HCl, stirred magnetically until the template was completely dissolved. 4.25 g of TEOS were then added slowly and stirred continuously to form a homogeneous solution. Stirring continued at 40 °C for 24 hours, after which it was crystallized in a polytetrafluoroethylene substrate reaction kettle at 100 °C for 48 hours. The resulting product was filtered, washed with deionized water, dried at room temperature, and finally calcined in a muffle furnace at 550 °C for 24 hours to remove the triblock copolymer. This yielded the mesoporous material SBA-15 molecular sieve, as a white powder.

2.3.2. Preparation of (SBA-15)-Hg(II)

0.167 g of $Hg(NO_3)_2{\cdot}0.5H_2O$ was dissolved in 1 L of deionized water. 40 mL of the Hg^{2+} standard solution were placed in a beaker, the pH was adjusted to 5 using 0.1 mol/L HNO_3 and NaOH solutions, and 0.10 g of SBA-15 was added and stirred for 40 minutes. The solution was filtered and dried at 25 $\pm$ 1 °C to obtain (SBA-15)-Hg(II).

2.3.3. Adsorption of S^{2-} by (SBA-15)-Hg(II)

The gravimetric method was used to measure and calculate the adsorption related parameters. 0.050 g of (SBA-15)-Hg(II) were added to 20 mL of 0. 2 mg-Na_2S/mL (conditional experiment: 0.04,0.1,0.2,0.6 mg-Na_2S/mL), and the pH adjusted to 9.5 (conditional experiment: 7, 8, 9, 9.5, 10, 11, 12). The solution volume was controlled to 40 mL by adding water and it was stirred at 25 $\pm$1 °C for 40 minutes (conditional experiment: 10, 20, 30, 35, 40, 45, 50 minutes). After centrifugation, the supernatant was titrated to excess with 0.1 mol/L $AgNO_3$ solution and, when precipitation was complete, subject to vacuum filtration and the product (SBA-15)-Hg(II)-S^{2-} dried at room temperature.

The precipitate mass produced was weighed and the residual S^{2-} concentration in the solution calculated. The amount of S^{2-} adsorbed by the modified SBA-15 was calculated by subtraction, and then the adsorption capacity and rate.

The equilibrium adsorption capacity, q_e, of S^{2-} and its adsorption capacity at time t, q_t, were obtained using Equations (1) and (2):

$$q_e = (C_0 - C_e)\cdot V/m \quad (1)$$

$$q_t = (C_0 - C_t)\cdot V/m \quad (2)$$

where C_0 is the initial adsorption concentration of the adsorbate, C_e the equilibrium adsorption concentration, C_t the adsorption concentration at time t, V the solution volume, and m the adsorbent mass. The C_0, C_e, C_t are measured in mg/ml, V in ml, and m in g.

2.3.4. Adsorption kinetics

0.050 g of (SBA-15)-Hg(II) was added to 20 mL of Na_2S solution at concentrations of 0.04, 0.1, 0.2 and 0.6 mg/mL. The pH was adjusted to 9.5 and water added to bring the volume to 40 mL, before adsorption took place at room temperature for known periods of time. After that the liquor was centrifuged and the supernatant was titrated with excess 0.1 mol-$AgNO_3$/L. When precipitation was complete, the product was subjected to vacuum filtration and dried at room temperature. The mass of Ag_2S precipitate was weighed and the residual S^{2-} concentration in solution calculated, so that the amount of S^{2-} adsorbed by the (SBA-15)-Hg(II) could be calculated by differential subtraction. Once q_e and q_t were calculated, quasi-first-order and quasi-second-order dynamic equations were obtained, and the corresponding parameters.

2.3.5. Adsorption isotherm

0.050 g of (SBA-15)-Hg(II) were added to 20 mL of Na_2S solution to yield concentrations of 0.04, 0.1, 0.2 and 0.6 mg/mL. The pH was adjusted to 9.5 and water added to bring the volume to 40 mL. Adsorption was carried out for known time periods at 25, 35 and 45 °C, after which the mixture was centrifuged, and the supernatant titrated with excess 0.1 mol/L $AgNO_3$ solution. The precipitate was vacuum filtered and dried at room temperature. The mass of precipitate was weighed and the residual S^{2-} concentration in solution calculated. From this, the amount of S^{2-} adsorbed by the (SBA-15)-Hg(II) was calculated by differential subtraction. When q_e and q_t were calculated, a quasi-first-order dynamic equation and Langmuir and Freundlich adsorption isotherms were drawn, and the corresponding parameters calculated.

3. RESULTS AND DISCUSSION

3.1. Effect of adsorption conditions

The effect of pH on the adsorbent's ability to sorb S^{2-} is very important. It can be seen in Figure 1 that when the solution pH is below 9.5, the amount adsorbed increases with increasing pH, and at pH 9.5, the modified material's adsorption rate and capacity are at their maxima. Thereafter, adsorption decreases with increasing pH.

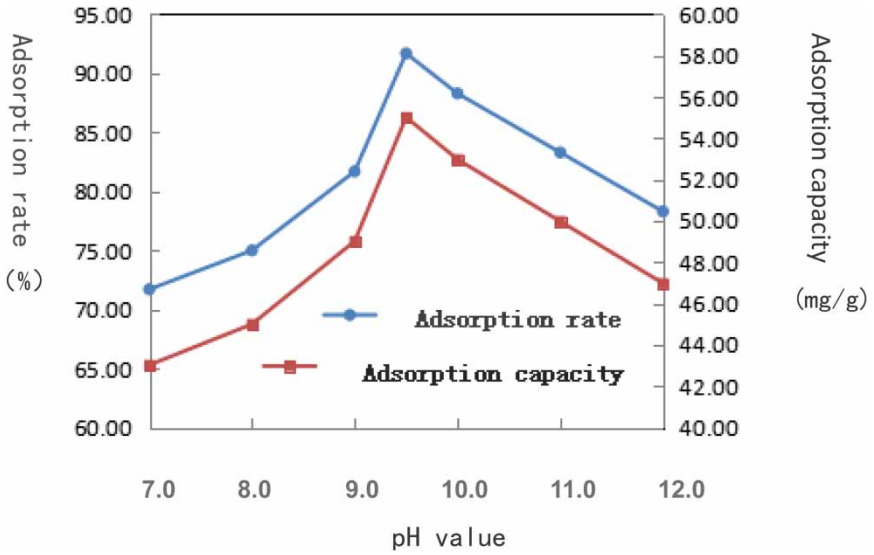

Figure 1 | Effect of pH on S^{2-}adsorption (adsorbent dosage: 1.67 g/L, contact time: 40 min, initial Na_2S concentration: 0.1 mg/mL, temperature: 25 °C).

When the pH is low, the adsorption sites of modified SBA-15 adsorb mainly sulfur ions. When it is too high, however, hydroxyl ions fight S^{2-} for adsorption sites, reducing their adsorption capacity.

The effect of different initial Na_2S solution concentrations on adsorption ability is shown in Figure 2. As the initial concentration of Na_2S increases, the adsorption capacity for S^{2-} increases gradually. The maximum adsorption rate occurs when the solution concentration reaches 0.10 mg-Na_2S/mL. When the concentration exceeds that, the adsorption rate decreases due to saturation of the adsorption sites.

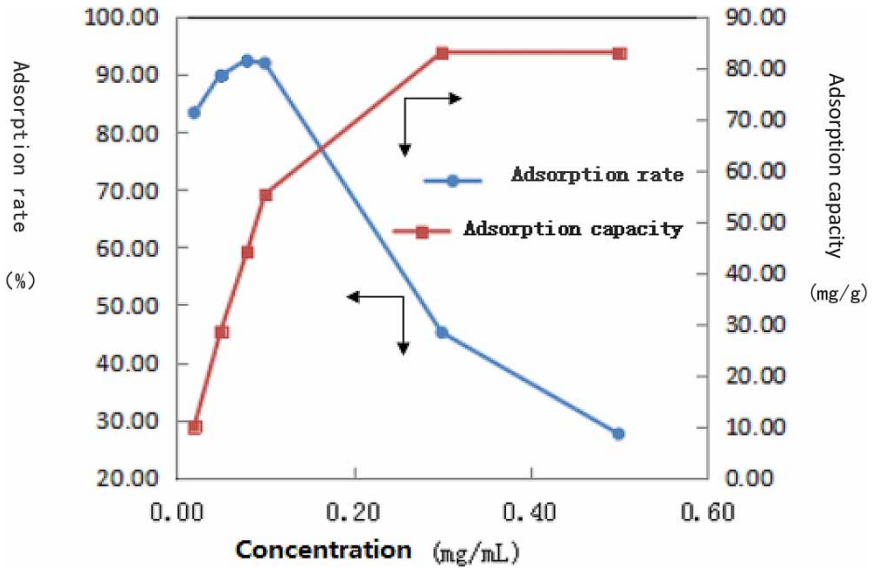

Figure 2 | Effect of initial Na_2S concentration on S^{2-} adsorption (adsorbent dosage: 1.67 g/L, contact time: 40 min, pH: 9.5, temperature: 25 °C).

The effect of contact time is shown in Figure 3. The adsorption rate and capacity increase significantly with increasing contact time, and reach the maximum at 40 minutes, after which both are stable.

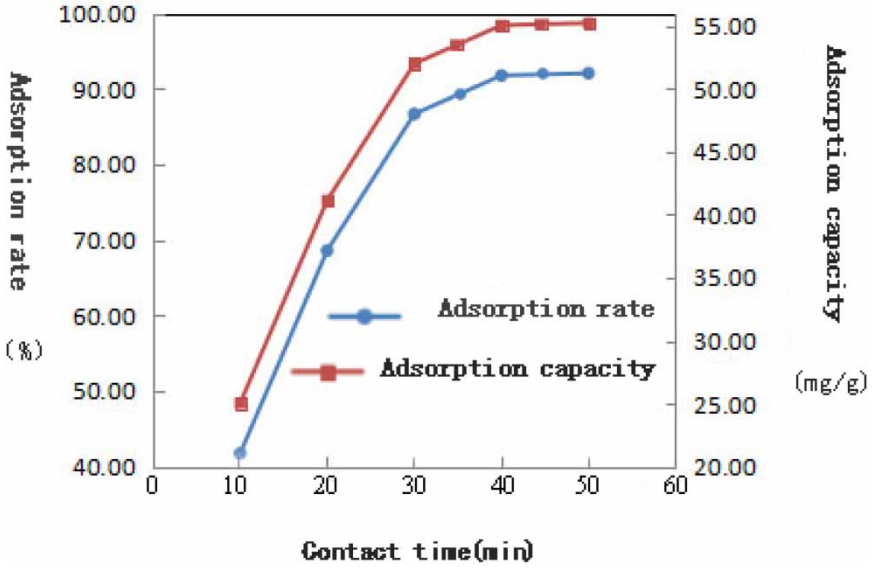

Figure 3 | Effect of contact time on S^{2-} adsorption (adsorbent dosage: 1.67 g/L, initial Na_2S concentration: 0.1 mg/mL, pH: 9.5, temperature: 25 °C).

The effects of temperature – observed at 298.15, 308.15, and 318.15 K – are shown in Figure 4. The adsorption rate decreases with increasing temperature, indicating that the adsorption process is exothermic.

3.2. Adsorption kinetics

Quasi-first-order and second-order dynamic equations were developed using the time and concentration data in linear fitting – see Figures 5 and 6, respectively. The dynamic data are listed in Table 1, where q_{e1}, q_{e2} are the theoretical q_e values obtained from the quasi-first and second-order dynamic equations, respectively, and R_1^2, R_2^2 are their respective correlation coefficients. It is clear that the S^{2-} adsorption process by (SBA-15)-Hg(II) is in better accord with the quasi-second-order kinetic equation than the first, the correlation coefficient being 0.9992, 0.9998 and 0.9997, respectively, and the difference between theoretical and actual q_e is small. However,

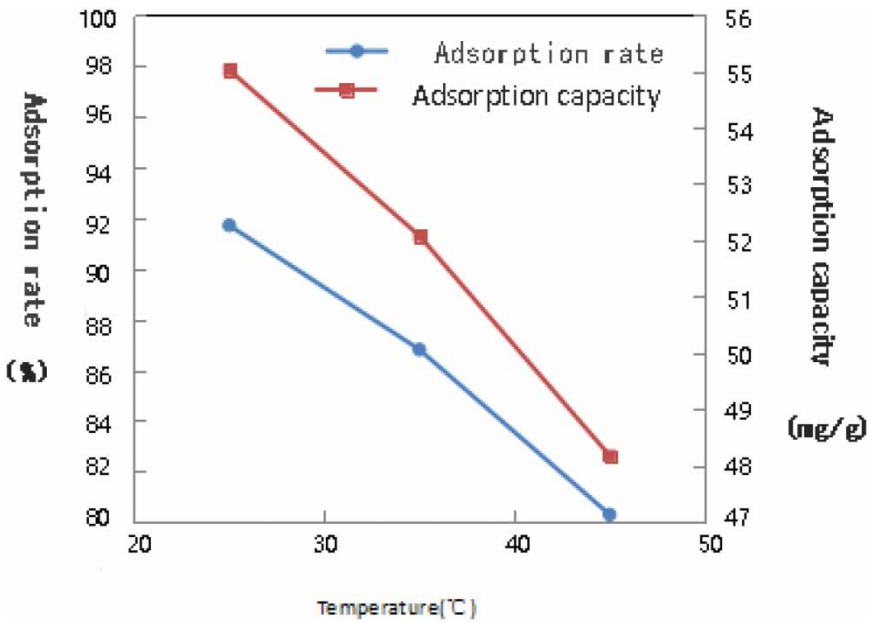

Figure 4 | Effect of temperature on S^{2-} adsorption (initial Na_2S concentration: 0.1 mg/mL, pH: 9.5, contact time: 40 min).

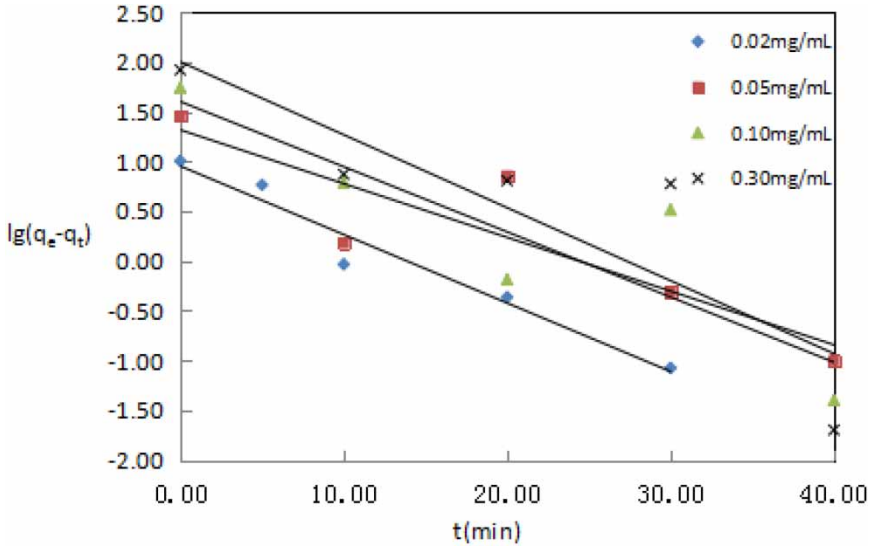

Figure 5 | Quasi-first-order dynamic equation (adsorbent dosage: 1.67 g/L, pH: 9.5, temperature: 25 °C).

most of the correlation coefficients for the quasi-first-order kinetic equation are around 0.78, when it is used to fit the adsorption process. The error is also larger and the theoretical q_e differs considerably from the actual q_e, indicating that the quasi-second-order kinetic equation expresses the S^{2-} adsorption process (SBA-15)-Hg(II) better.

3.3. Adsorption isotherm

The adsorption data were investigated in relation to the Langmuir and Freundlich adsorption isotherms. The linear Equation – (3) – for the Langmuir isotherm is (Langmuir 1916, 1918; Crini *et al.* 2007; Naushad 2014; Alqadami *et al.* 2017):

$$\frac{C_e}{q_e} = \frac{1}{Q_0 b} + \left(\frac{1}{Q_0}\right) C_e \tag{3}$$

where C_e/q_e (g/mL) is the equilibrium constant, C_e (mg/mL) the adsorbate's equilibrium concentration, and q_e the adsorption capacity – that is the mass by the adsorbent per unit mass. Q_0 (mg/mL) and b (mL/mg) represent the relationship among the Langmuir constant and the adsorption capacity and rate, respectively.

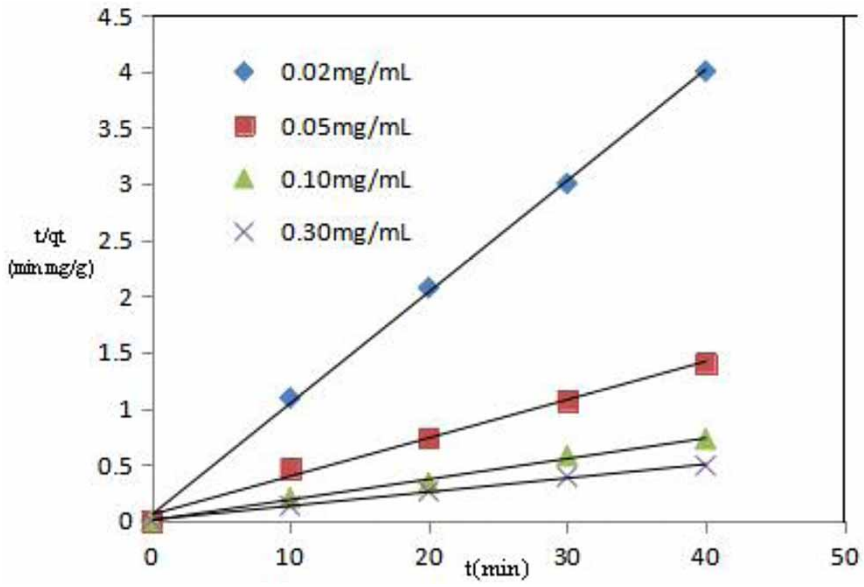

Figure 6 | Quasi-second-order kinetic equation (adsorbent dosage: 1.67 g/L, pH: 9.5, temperature: 25 °C).

Table 1 | Adsorption kinetics parameters

		Quasi-first-order adsorption kinetic equation			Quasi-second-order adsorption kinetic equation		
Concentration (mg/mL)	Actual measurement q_e (mg/g)	$k_1(min^{-1})$	q_{e1}	R_1^2	$k_2(min^{-1})$	q_{e2}	R_2^2
0.02	10.1	0.1584	8.97	0.9578	0.1922	10.1	0.9992
0.05	28.6	0.1243	20.97	0.7876	0.0217	29.3	0.9928
0.10	55.3	0.1508	39.9	0.7827	0.1082	54.6	0.9937
0.30	83.0	0.1688	100.0	0.7517	0.0213	80.6	0.9975

The linear equation – (4) – for the Freundlich isotherm is (Freundlich 1906; Langmuir 1916, 1918):

$$\ln q_e = \ln K_F + \frac{1}{n}\ln C_e \tag{4}$$

where q_e (mg/g) is the adsorption capacity at equilibrium, C_e (mg/mL) the absorbate concentration at equilibrium. K_F is the Freundlich adsorption isotherm constant (the coefficient of adsorption degree) and *1/n* – usually <1 – indicates adsorption intensity.

The results of simulating the Langmuir and Freundlich adsorption isotherms are shown in Figures 7 and 8, respectively. The related parameters are listed in Table 2. As can be seen, the S^{2-} adsorption process by (SBA-15)-Hg(II) is closer to the Freundlich isotherm and R^2 is 0.9951, 0.9906, 0.9914 – that is it always exceeds 0.99. All values of 1/n are below 1, too, indicating S^{2-} adsorption by (SBA-15)-Hg(II) is preferential.

3.4. Adsorption thermodynamics

The Gibbs free energy in the reaction (ΔG^0), and the enthalpy (ΔH^0) and entropy (ΔS^0) changes are obtained using equations 5, 6 and 7 respectively (Chowdhury *et al.* 2011; Zhou *et al.* 2013; Naushad *et al.* 2016):

$$K_d = q_e/C_e \tag{5}$$

$$\ln K_d = -\Delta H/(RT) + \Delta S/R \tag{6}$$

$$\Delta G^0 = \Delta H^0 - T\Delta S^0 \tag{7}$$

where K_d (K) is the temperature-dependent adsorption equilibrium constant, ΔG^0 is the free energy change during adsorption (kJ/mol), ΔH^0 the enthalpy change during adsorption (kJ/mol), R the ideal gas constant (8.314J·mol^{-1}·K^{-1}), T the absolute temperature (K), and ΔS^0 the entropy change during adsorption (J/mol·K).

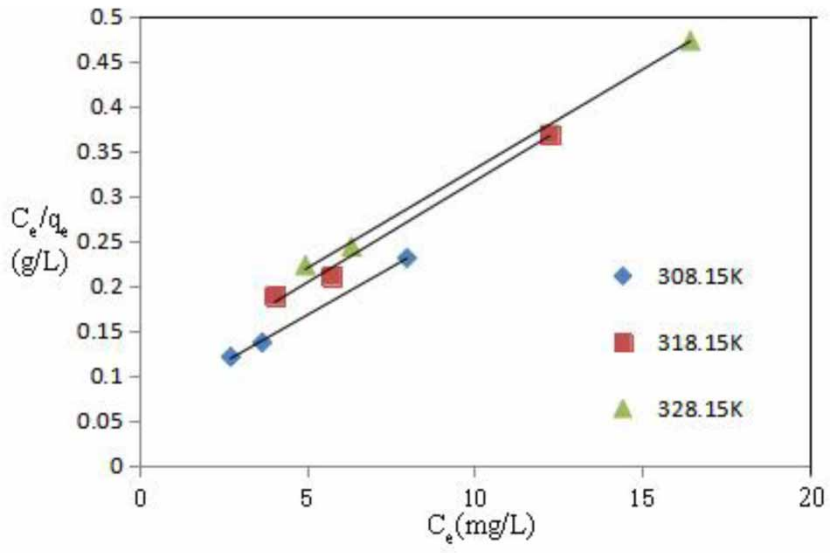

Figure 7 | Langmuir adsorption isotherm (adsorbent dosage: 1.67 g/L, pH: 9.5).

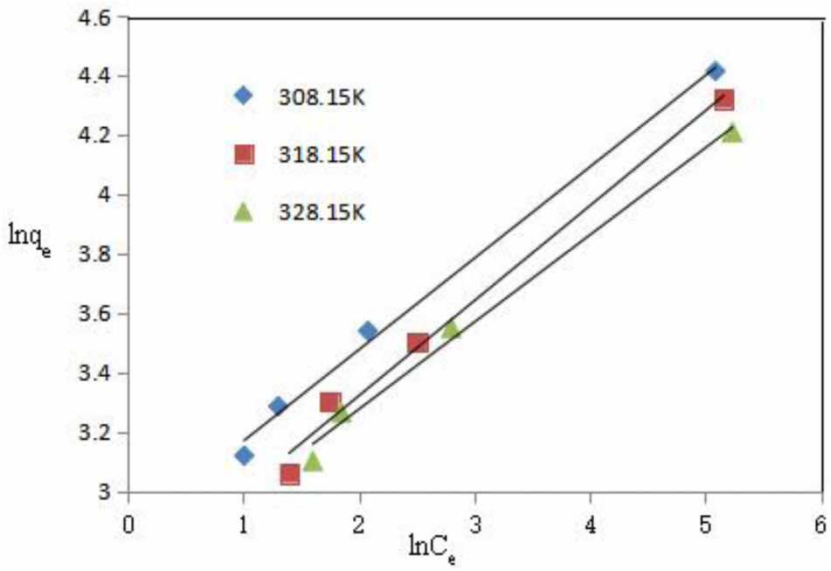

Figure 8 | Freundlich adsorption isotherm (adsorbent dosage: 1.67 g/L, pH: 9.5).

Table 2 | Adsorption isotherm parameters

	Langmuir adsorption isotherm			Freundlich adsorption isotherm		
Temperature/K	q_o	b	R^2	K_F(L/g)	1/n	R^2
308.15	47.39	0.3431	0.9869	17.49	0.3074	0.9951
318.15	39.22	0.2808	0.9730	14.65	0.3196	0.9906
328.15	45.25	0.2026	0.9888	41.20	0.2930	0.9914

The calculated adsorption thermodynamic parameters are shown in Table 3. At and above room temperature (308.15–328.15 K), $\Delta G^0 < 0$, showing that adsorption is spontaneous. The value of ΔG^0 is between 0 and −20 kJ/mol, indicating that adsorption is physical (Gerçel *et al.* 2007). $\Delta H^0 = -28.561$ kJ/mol ($\Delta H^0 < 0$),

Table 3 | Adsorption thermodynamics parameters

Temperature/K	ΔG^0 (kJ/mol)	ΔH^0 (kJ/mol)	ΔS^0 (J/(mol·K))
308.15	−3.558	− 28.561	− 81.136
318.15	−2.746		
328.15	−1.935		

which shows that S^{2-} adsorption by (SBA-15)-Hg(II) is exothermic. $\Delta S^0 = -81.136$ J/(mol·K), ($\Delta H^0 < 0$), indicating that the process reduces entropy.

3.5. Characterization of SBA-15 related material

Figures 9 and 10 show the small and wide angle XRD images, respectively, of SBA-15, (SBA-15)-Hg(II), the (SBA-15)-Hg(II) with S^{2-} adsorbed. The XRD small angle image of the SBA-15 molecular sieves has four peaks (Zhai 2012), which can be assigned to those obtained by (100), (110), (200) and (210) crystal plane diffraction, respectively. The peaks confirm that the SBA-15 prepared is a molecular sieve. In the wide-angle images, the (SBA-15)-Hg(II) peak is unchanged but the peak is lower, showing that modification was successful and caused no damage to the original SBA-15 skeleton. The characteristic diffraction peaks of SBA-15 exist after S^{2-} adsorption by (SBA-15)-Hg(II), proving that the original SBA-15 framework is still present.

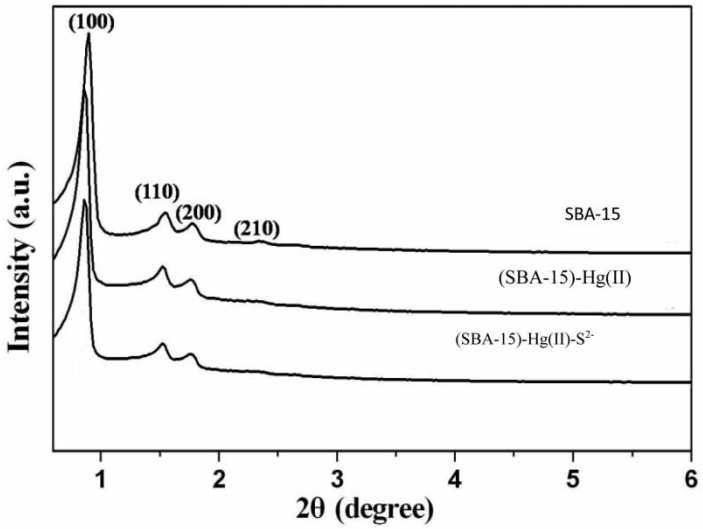

Figure 9 | Small-angle XRD images.

Figure 11 shows the SEM images of SBA-15, (SBA-15)-Hg(II), S^{2-} adsorbed (SBA-15)-Hg(II), respectively. As can be seen, the grain fiber diameter of the three materials is 333, 360, and 350 nm, respectively. The SBA-15 molecular sieve has a rod-like structure, and, after adsorption, the crystallinity decreases and the disorder increases.

Figure 12 shows the nitrogen adsorption-desorption isotherms at low temperature, and the typical type IV adsorption isotherms in the IUPAC (International Union of Pure and Applied Chemistry) classification, with the H1 lag rings characteristic of typical mesoporous materials. The mesoporous properties were determined using the adsorption data: total surface area and pore volume, and the pore diameter in the BJH model (Barrett *et al.* 1951). When the relative pressure is below 0.6, the adsorption process exhibits linear correlation. The sudden increase at about 0.65, and sharp increase in the volume of nitrogen adsorbed, are characteristic of capillary condensation in the mesopores. The curve tends to be flat after about 0.8. These characteristics show that the adsorption of S^{2-} resulted in decreases in mesoporous area and pore volume.

Table 4 is a summary of the physicochemical characteristics of the SBA-15 in the three samples. The three samples showed similar inflection points, tending to lower relative pressure with Hg^{2+} modification and subsequent S^{2-} adsorption. A sequential decrease in specific surface was observed for the three samples, which

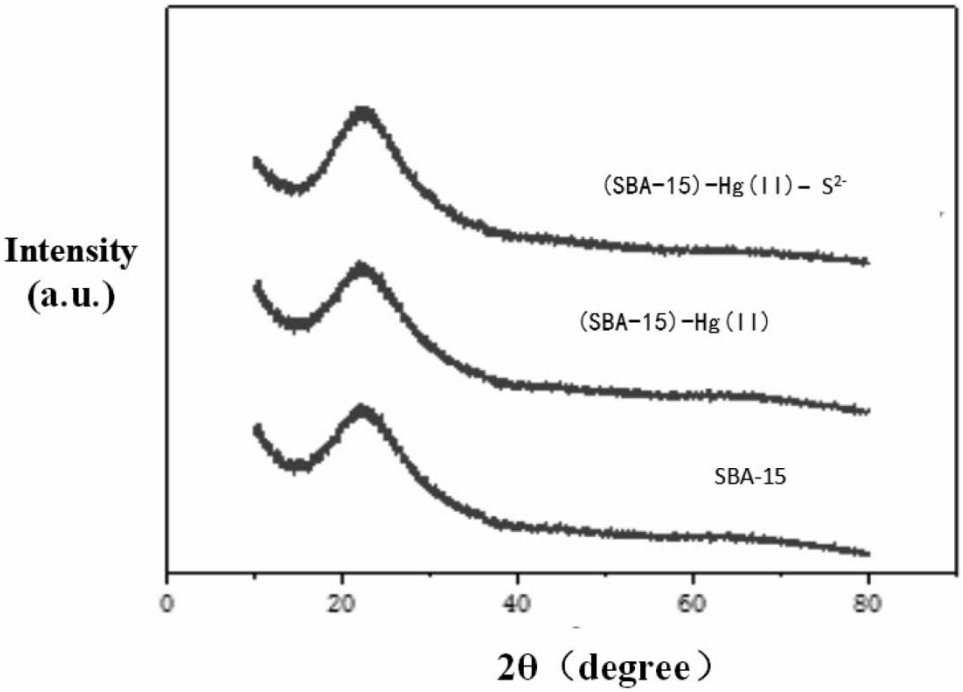

Figure 10 | Wide-angle XRD images.

occurred because the guest molecules adsorbed stayed and were tightly packed within the SBA-15 porous network.

As can be seen in Figure 13, the pore size distribution of the three samples is very narrow, indicating that they all have a regular and single mesoporous framework structure (the samples' pore size structure parameters are given in Table 4). It can be concluded from Figure 13 and Table 4 that Hg^{2+} modification and subsequent S^{2-} adsorption do not change the original SBA-15 structure. The pore wall thickness increases gradually with increasing ionic adsorption. The reductions in BET surface area, mesoporous volume and average pore size all show that after adsorbing S^{2-} the SBA-15 channel was partially filled and blocked, indicating that S^{2-} has been adsorbed in SBA-15 channels.

4. CONCLUSIONS

Nano-mesoporous SBA-15 was synthesized successfully using a hydrothermal method. The adsorption conditions and kinetics, adsorption isotherms and thermodynamic-related properties of S^{2-} adsorption by (SBA-15)-Hg(II) were studied. XRD images were taken after adsorption. The post-adsorption materials were also characterized by SEM and low-temperature (77 K) nitrogen adsorption-desorption. It was concluded that:

(1) The optimum adsorption conditions for S^{2-} by (SBA-15)-Hg(II) are: 1.67 g-SBA-15/L, pH 9.5, temperature and time 25 °C for 40 minutes. The maximum adsorption efficiency and capacity were about 92% and 55.02 mg/g, respectively.
(2) The adsorption of S^{2-} by (SBA-15)-Hg(II) is best fitted by the quasi-second-order kinetic equation, and the adsorption isotherm is best fitted by the Freundlich model.
(3) Thermodynamically, the entropy and Gibbs free energy changes for S^{2-} adsorption by (SBA-15)-Hg(II) are all below zero, indicating that the process is exothermic and accompanied by a decrease in entropy.

ACKNOWLEDGEMENTS

This study was funded by the Natural Science Foundation of the Department of Science and Technology, from the Science and Technology Development Program of Jilin Province, P. R. China. The project number was 20180101180JC, 222180102051, KYC-JC-XM-2018-051. This study was supported by Science Research Project of Education Department, Jilin Province from the 13th Five-Year Plan (JJKH20200265KJ). The authors would like to express their thanks.

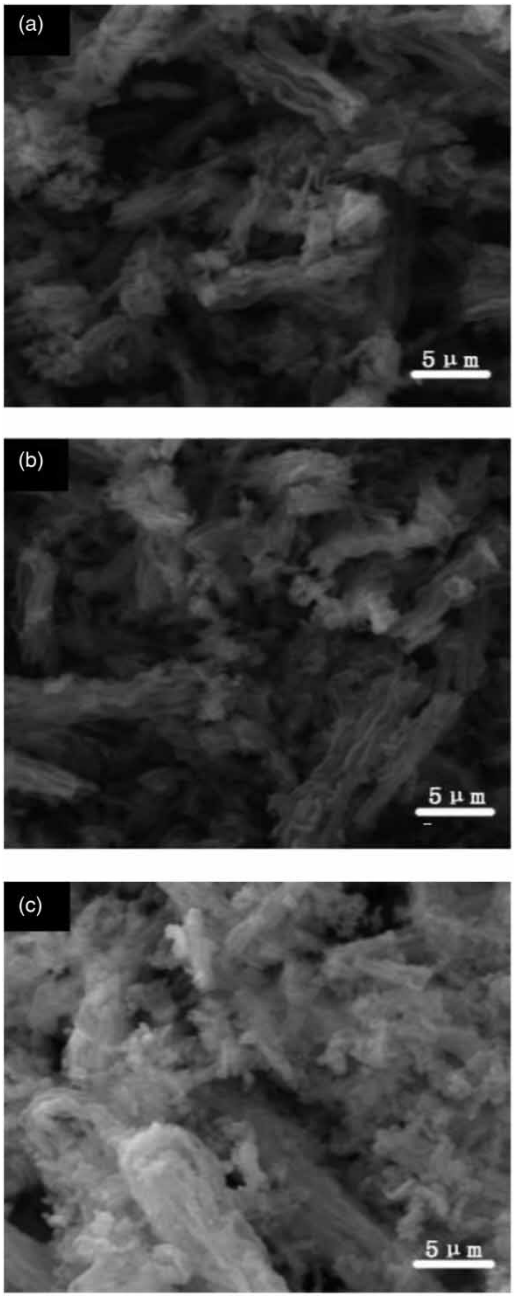

Figure 11 | SEM images of (a) SBA-15, (b) (SBA-15)-Hg(II), (c) (SBA-15)-Hg(II) adsorbed S^2.

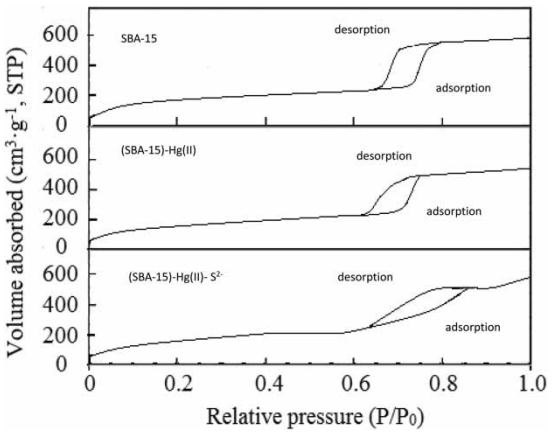

Figure 12 | Nitrogen adsorption-desorption curves.

Table 4 | Pore size structure parameters

Sample	Interplanar spacing d_{100} (nm)	Cell parameters a_0 (nm)	Wall thickness (nm)	BET surface area (m^2/g)	Mesopore volume (cm^2/g)	Mean pore diameter (nm)
SBA-15	10.26	11.85	4.15	613	1.04	7.70
(SBA-15)-Hg(II)	10.33	11.94	4.61	587	0.94	7.33
(SBA-15)-Hg(II)-S^{2-}	10.43	12.05	4.76	503	0.85	7.29

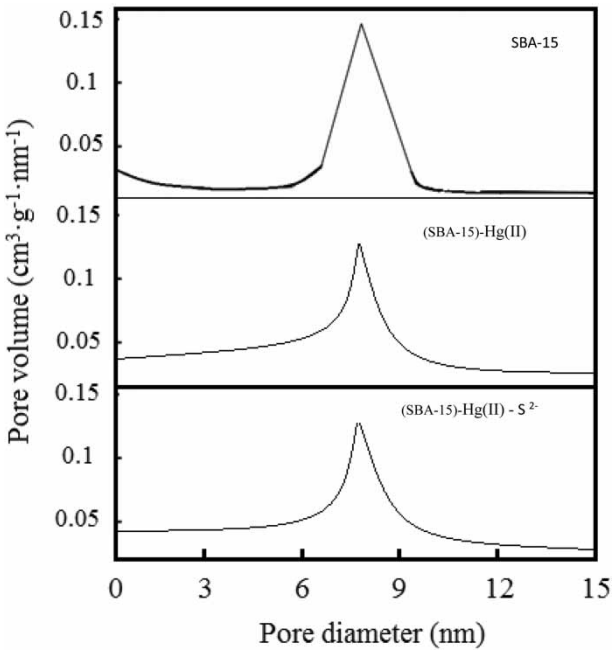

Figure 13 | Pore size distribution patterns.

CONFLICT OF INTEREST

The authors declare that they have no conflict of interest.

DATA AVAILABILITY STATEMENT

All relevant data are included in the paper or its Supplementary Information.

REFERENCES

Alqadami, A. A., Naushad, M., Alothman, Z. A. & Ghfar, A. A. 2017 Novel metal-organic framework (MOF) based composite material for the sequestration of U(VI) and Th(IV) metal ions from aqueous environment. *ACS Applied Materials & Interfaces* **9**(41), 36026–36037. https://doi.org/10.1021/acsami.7b10768.

Barrett, E. P., Joyner, L. G. & Halenda, P. P. 1951 The determination of pore volume and area distributions in porous substances. I. computation from nitrogen isotherms. *Journal of American Chemical Society* **73**(1), 373–380. https://doi.org/10.1021/ja01145a126.

Broekhoff, J. C. P. & De Boer, J. H. 1968a Studies on pore systems in catalysts: XI. Pore distribution calculations from the adsorption branch of a nitrogen adsorption isotherm in the case of 'ink-bottle' type pores. *Journal of Catalysis* **10**(2), 153–165. https://doi.org/10.1016/0021-9517(68)90168-1.

Broekhoff, J. C. P. & De Boer, J. H. 1968b Studies on pore systems in catalysts: XII. Pore distributions from the desorption branch of a nitrogen sorption isotherm in the case of cylindrical pores A. An analysis of the capillary evaporation process. *Journal of Catalysis* **10**(4), 391–400. https://doi.org/10.1016/0021-9517(68)90152-8.

Brunauer, S., Emmett, P. H. & Teller, E. 1938 Adsorption of gases in multimolecular layers. *Journal of American Chemical Society* **60**(2), 309–319. https://doi.org/10.1021/ja01269a023.

Castillo, X., Pizarro, J., Ortiz, C., Cid, H. & Voort, P. V. D. 2018 A cheap mesoporous silica from fly ash as an outstanding adsorbent for sulfate in water. *Microporous & Mesoporous Materials* **272**, 184–192. https://doi.org/10.1016/j.micromeso.2018.06.014.

Chang, X. Q., Wang, W. S., Liu, B. S., Huang, L. Z. & Han, F. S. 2018 One-step strategic synthesis of x%Ni–AlSBA-15 sorbents and properties of high adsorption desulfurization for model and commercial liquid fuels. *Microporous & Mesoporous Materials* **268**, 276–284. https://doi.org/10.1016/j.micromeso.2018.04.027.

Chowdhury, S., Mishra, R., Saha, P. & Kushwaha, P. 2011 Adsorption thermodynamics, kinetics and isosteric heat of adsorption of malachite Green onto chemically modified ice husk. *Desalination* **265**(1–3), 159–168. https://doi.org/10.1016/j.desal.2010.07.047.

Crini, G., Peindy, H. N., Gimbert, F. & Robert, C. 2007 Removal of C. I. basic Green 4 (malachite Green) from aqueous solution by adsorption using cyclodextrin-based adsorbent: kinetic and equilibrium studies. *Separation & Purification Technology* **53**(1), 97–110. https://doi.org/10.1016/j.seppur.2006.06.018.

Diagboya, P. N. E. & Dikio, E. D. 2018 Silica-based mesoporous materials; emerging designer adsorbents for aqueous pollutants removal and water treatment. *Microporous & Mesoporous Materials* **266**, 252–267. https://doi.org/10.1016/j.micromeso.2018.03.008.

Dido, C. A., Caneppele, C. D. G., Schneid, A. C., Pereira, M. B. & Benvenutti, E. V. 2018 Small gold nanoparticles with narrow size distribution achieved in SBA-15 pores by using ionic silsesquioxane instead of thiol group as stabilizer and adhesion agent. *Microporous & Mesoporous Materials* **270**, 48–56. https://doi.org/10.1016/j.micromeso.2018.04.047.

Freundlich, H. 1906 Uber die adsorption in losungen (Over the adsorption in solution). *Zeitschift fur Physikalische Chemie* **57**, 385–470. https://doi.org/10.1515/zpch-1907-5723.

Gerçel, O., Ozcan, A., Ozcan, A. S. & Gercel, H. F. 2007 Preparation of activated carbon from a renewable bio-plant of Euphorbia rigida, by H_2SO_4, activation and its adsorption behavior in aqueous solutions. *Applied Surface Science* **253**(11), 4843–4852. https://doi.org/10.1016/j.apsusc.2006.10.053.

Kanga, J.-K., Lee, S.-C. & Kim, S.-B. 2018 Enhancement of selective Cu(II) sorption through preparation of surface-imprinted mesoporous silica SBA-15 under high molar concentration ratios of chloride and copper ions. *Microporous & Mesoporous Materials* **272**, 193–201. https://doi.org/10.1016/j.micromeso.2018.06.038.

Lakhi, K. S., Singh, G., Kim, S., Baskar, A. V. & Vinu, A. 2018 Mesoporous Cu-SBA-15 with highly ordered porous structure and its excellent CO_2 adsorption capacity. *Microporous & Mesoporous Materials* **268**, 134–141. https://doi.org/10.1016/j.micromeso.2018.03.024.

Langmuir, I. 1916 The constitution and fundamental properties of solids and liquids. *Journal of the American Chemical Society* **38**, 2221–2295. https://doi.org/10.1021/ja02268a002.

Langmuir, I. 1918 Adsorption of gases on plain surfaces of glass mica platinum. *Journal of the American Chemical Society* **40**, 1361–1403. https://doi.org/10.1016/s0016-0032(17)90938-x.

Mikheeva, N. N., Zaikovskii, V. I. & Mamontov, G. V. 2019 Synthesis of ceria nanoparticles in pores of SBA-15: pore size effect and influence of citric acid addition. *Microporous & Mesoporous Materials* **277**, 10–16. https://doi.org/10.1016/j.micromeso.2018.10.013.

Naushad, N. 2014 Surfactant assisted nano-composite cation exchanger: development, characterization and applications for the removal of toxic Pb^{2+} from aqueous medium. *Chemical Engineering Journal* **235**, 100–108. https://doi.org/10.1016/j.cej.2013.09.013.

Naushad, M., Ahamad, T., Sharma, G., Al-Muhtaseb, A. H., Albadarin, A. B., Alam, M. M., Alothman, Z. A., Alshehri, S. M. & Ghfar, A. A. 2016 Synthesis and characterization of a new starch/SnO_2 nanocomposite for efficient adsorption of toxic Hg^{2+} metal ion. *Chemical Engineering Journal* **300**, 306–316. https://doi.org/10.1016/j.cej.2016.04.084.

Nazal, M. K., Rao, D. & Abuzaid, N. 2021 First investigations on removal of nitrazepam from water using biochar derived from macroalgae low-cost adsorbent: kinetics, isotherms and thermodynamics studies. *Water Practice and Technology* **16**(3), 946–960. https://doi.org/10.2166/wpt.2021.040.

Pirez, C., Morin, J. C., Manayil, J. C., Lee, A. F. & Wilson, K. 2018 Sol-gel synthesis of SBA-15: impact of HCl on surface chemistry. *Microporous & Mesoporous Materials* **271**, 196–202. https://doi.org/10.1016/j.micromeso.2018.05.043.

Szewczyk, A., Prokopowicz, M., Sawicki, W., Majda, D. & Walker, G. 2019 Aminopropyl- functionalized mesoporous silica SBA-15 as drug carrier for cefazolin: adsorption profiles, release studies, and mineralization potential. *Microporous & Mesoporous Materials* **274**, 113–126. https://doi.org/10.1016/j.micromeso.2018.07.046.

Wang, K. J. & Hu, C. 2006 Biological sulfur cycle and new development in desulfurization technology. *Environmental Protection* **2**, 69–72. doi: 10.3969/j.issn.0253-9705.2006.02.016.

Wu, H. F., Wang, P., Wang, Z. Q., Sun, Y. F., Li, C. L. & Dong, Y. C. 2021 Preparation of EDTA modified cotton fiber iron complex and catalytic properties for aqueous Cr(VI) reduction and dye degradation. *Water Practice and Technology* **16**(3), 1000–1011. https://doi.org/10.2166/wpt.2021.047.

Zhai, Q. Z. 2012 Inclusion of cefalexin in SBA-15 mesoporous material and release property. *Materals Science Engineering: C* **32**(8), 2411–2417. https://doi.org/10.1016/j.msec.2012.07.015.

Zhai, Q. Z. 2020 Study on SBA-15 as an effective sorbent for dye butyl rhodamine B. *Journal of Sol-Gel Science & Technology* **96**, 34–46. https://doi.org/10.1007/s10971-020-05335-7.

Zhai, Q. Z., Ma, Y. Q., Yu, H. & Liu, X. H. 2011 SBA-15 for effective removal of mercury(II) from aqueous solution. *Asian Journal of Chemistry* **23**(9), 4079–4086.

Zhou, Y. M., Zhang, M., Hu, X. Y., Wang, X. H., Niu, J. Y. & Ma, T. S. 2013 Adsorption of cationic dyes on a cellulose-based multicarboxyl adsorbent. *Journal of Chemical & Engineering Data* **58**(2), 413–421. https://doi.org/10.1021/je301140c.

First received 30 June 2021; accepted in revised form 13 August 2021. Available online 25 August 2021